Effect of electrical boundary conditions on ferroelectric domain structures in thin films

Y. L. Li, S. Y. Hu, Z. K. Liu, and L. Q. Chen[a)]
Department of Materials Science and Engineering, The Pennsylvania State University, University Park, Pennsylvania 16802

(Received 6 July 2001; accepted for publication 14 May 2002)

The domain structures in a ferroelectric thin film are studied using a phase-field model. A cubic-to-tetragonal ferroelectric phase transition in lead titanate thin film is considered. Both elastic interactions and electrostatic interactions are taken into account. The focus is on the effect of electrical boundary conditions on the domain morphologies and volume fractions. It is shown that different electric boundary conditions may have a significant effect on the domain structures. © *2002 American Institute of Physics.* [DOI: 10.1063/1.1492025]

Ferroelectric thin films find potential applications in many electronic and electro-optical devices including nonvolatile memories, thin film capacitors, sensors, etc.[1–3] The crystallography and thermodynamics of domain structures in ferroelectric thin films have been extensively studied.[4–17] A given domain structure with a particular domain wall orientation was usually assumed as *a priori* in these theoretical analyses. Recently we showed that the phase-field approach could be employed to predict the domain structures in constrained three-dimensional ferroelectric thin films without any *a priori* assumptions with regard to the possible domain structures.[18,19] It is able to predict not only the effect of substrate constraint on phase transition temperatures and the volume fractions of different orientation domains, but also the detailed domain structures and their temporal evolution during a ferroelectric transition. In this letter, we study the effect of the electric boundary conditions on the domain structures by extending the phase-field approach[18,19] to include the electrostatic interactions.

A cubic thin film grown heteroepitaxially on a cubic substrate is considered. The film undergoes ferroelectric phase transitions from the cubic paraelectric phase when it is cooled below the Curie temperature. The domain structure is described by the spatial distribution of local polarization $\mathbf{P(x)}=(P_1,P_2,P_3)$, where $\mathbf{x}=(x_1,x_2,x_3)$ is a rectangular coordinate system originated at the film-substrate interface with x_3 normal to the film. The electric energy density of a given polarization distribution is calculated by

$$f_{\text{elec}}=-\tfrac{1}{2}E_i(\varepsilon_0\kappa_{ij}E_j+P_i)\equiv f_{\text{elec}}(P_i,E_i), \tag{1}$$

where E_i is the electric field component. It is related to the electric displacement D_i through the usual relation, $D_i=\varepsilon_0\kappa_{ij}E_j+P_i$, in which, $\varepsilon_0=8.85\times10^{-12}$ F m^{-1} is known as the dielectric permittivity of a vacuum, and κ_{ij} is the relative dielectric permittivity. The summation convention for the repeated indices is employed in this letter and the subscripts *i,j* run from 1 to 3.

Suppose there is no space charge inside the film, the electric displacement, D_i satisfies the electrostatic equilibrium equation of $D_{i,i}=0$ in the film, where the comma in the subscript stands for spatial differentiation. On the top and bottom surfaces of the film

$$D_3|_{x_3=0,h_f}=0 \tag{2}$$

for an open-circuit condition, or

$$\phi|_{x_3=0}=\phi_1,\phi|_{x_3=h_f}=\phi_2 \tag{3}$$

if the electric potential, ϕ, is specified on both surfaces of the film, where h_f is the film thickness. ϕ is related to E_i through $E_i=-\phi_{,i}$. Thus, by assuming $\kappa_{ij}=0$ when $i\neq j$, the electrostatic equilibrium equation is given by

$$\kappa_{11}\phi_{,11}+\kappa_{22}\phi_{,22}+\kappa_{33}\phi_{,33}=\frac{1}{\varepsilon_0}(P_{1,1}+P_{2,2}+P_{3,3}). \tag{4}$$

For a given polarization distribution, to obtain the electric field components E_i and the electric displacements D_i, we employed the same methodology to solve the electrostatic equilibrium equation as that used in solving the elastic equilibrium equations in Ref. 19.

The total free energy of a film in a diffuse-interface description is then given by

$$F=\int_V[f_{\text{bulk}}(P_i)+f_{\text{grad}}(P_{i,j})+f_{\text{elas}}(P_i,\epsilon_{ij}) + f_{\text{elec}}(P_i,E_i)]d^3x, \tag{5}$$

where f_{bulk}, f_{grad}, f_{elas} and f_{elec} are the bulk chemical, gradient, elastic, and electric energy density, respectively, and V is the volume of the film. The mathematical expressions for the Landau bulk free (or bulk chemical) energy and the gradient energy are exactly the same as those given in Refs. 18 and 19. The calculation of the elastic energy is also described in detail in Ref. 19. In this work, we ignore any possible surface and interface contributions to the energy as discussed in Refs. 20 and 21. We assume that the mechanical and electric equilibriums are established instantaneously for a given polarization field distribution.

The temporal evolution of the polarization vector field is described by the time-dependent Ginzburg–Landau equations

a)Electronic mail: lqc3@psu.edu.

$$\frac{\partial P_i(\mathbf{x},t)}{\partial t} = -L\frac{\delta F}{\delta P_i(\mathbf{x},t)}, \tag{6}$$

where L is the kinetic coefficient related to the domain-wall mobility. Equation (6) is solved by employing the semi-implicit Fourier-spectral method.[22]

We consider lead titanate ($PbTiO_3$) thin film as an example for numerical simulation. The coefficients of the Landau free energy expansion and the electrostrictive and elastic constants are exactly the same as those given in Ref. 19, and they are adapted from the literature.[23,24] The relative dielectric permittivity is taken as $\kappa_{11}=\kappa_{22}=\kappa_{33}=66.0$.[23] In the computer simulations, we employ a $192\times192\times40$ discrete grid points and periodic boundary conditions are applied along the x_1 and x_2 axes. The grid spacing in real space is chosen to be $\Delta x_i/l_0=\Delta x/l_0=1.0$, where $l_0=\sqrt{G_{110}/\alpha_0}$ and $\alpha_0=1.7252\times10^8$ ($C^{-2}\,m^2\,N$). We choose the gradient energy coefficients as $G_{11}/G_{110}=2.0$, $G_{12}/G_{110}=0.0$, $G_{44}/G_{110}=G'_{44}/G_{110}=1.0$. The corresponding width of domain wall is about $2.5\Delta x$, and the domain wall energy densities at $T=25\,^\circ$C are evaluated to be about $1.22\alpha_0 l_0 P_0^2$ for 90° domain walls and $2.46\alpha_0 l_0 P_0^2$ for 180° domain walls, respectively. $P_0=|\mathbf{P}|_{T=25\,^\circ\mathrm{C}}=0.757\ \mathrm{C\,m^{-2}}$ is the spontaneous polarization. The time step for integration is $\Delta t/t_0=0.08$, where $t_0=1/(\alpha_0 L)$.

In this letter, we focus on the coupling effect of electrostatic boundary conditions and substrate constraint on the domain structures. In the simulation, two electrostatic conditions, (2) (open-circuit) and (3) at $\phi_1=\phi_2=$const (short circuit), are considered. The macroscopic constraint of the substrate is described by the average strain $\bar{\epsilon}_{\alpha\beta}(\alpha,\beta=1,2)$ while the continuities of the deformation and stresses on film-substrate interface provide the local/microscopic constraint. For a simple case—a thin film grown epitaxially on (001) cubic substrate, the average strains are of the form $\bar{\epsilon}_{11}=\bar{\epsilon}_{22}=\bar{\epsilon}$ and $\bar{\epsilon}_{12}=0$. We take the thickness of the film as $h_f=24\Delta x$ and allow the heterogeneous elastic deformation in the substrate by choosing a value of $h_s=14\Delta x$, where h_s is the distance from the interface into the substrate, beyond which our simulations showed little changes in the results.

Since the phase transition is from cubic to tetragonal, there are three possible orientation variants in the film with the tetragonal axes along the [100], [010] and [001] directions of the cubic paraelectric phase, respectively. They are labeled by a_1, a_2, and c, respectively. The polarization vector takes $\mathbf{P}=(P_1,0,0)$ in a_1 domain, $\mathbf{P}=(0,P_2,0)$ in a_2 domain, and $\mathbf{P}=(0,0,P_3)$ in c domain. Thus, we present the domain structures with the polarization vector components in a normalized form of $P_i^*=|P_i|/P_0$.

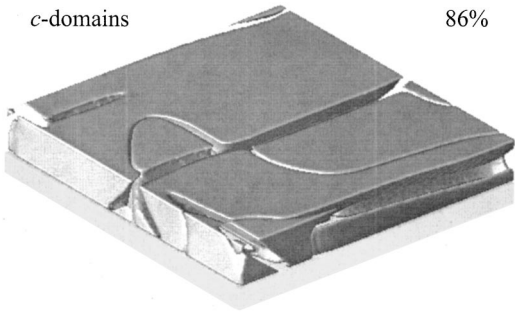

FIG. 2. Domain morphologies with $\bar{\epsilon}=-0.002$ and short-circuit electric condition.

First, to compare the domain structures under the two different electric boundary conditions, we consider a thin film under a compressive constraint of $\bar{\epsilon}=-0.002$ at a quenching temperature $T=25\,^\circ$C. We started the simulation from a homogeneous paraelectric phase created by assigning a zero value at each grid point for each component of the polarization field plus a small random noise of uniform distribution. The morphologies of the c domain structures near equilibrium are shown in Fig. 1 for the open-circuit boundary condition, Fig. 2 for the short-circuit boundary condition, and Fig. 3 without considering the electrostatic interaction at all (equivalent to assuming all the polarization charges on the surfaces and domain walls are compensated by free charges). The morphologies are the contours of $P_i^*=0.6$. The values in the figures are the corresponding c domain volume fractions. The a domains occupy the rest space of the simulation cell. As expected, the compressive substrate constraint favors the formation of c domains, and hence, the volume fraction of c domains is larger than that of a domains for all three cases. However, the incorporation of the dipole–dipole interactions and of different electric boundary conditions has a significant effect on the domain morphology and arrangement. In the case of open-circuit boundary condition (Fig. 1), the depolarization field caused by surface charge produces two effects. First, the depolarization field favors the formation of a domains over c domains near the surfaces, resulting in an increase in the volume fraction of a domains. Second, it leads to the refinement of size of the c domains, and the formation of neighboring c domains with antiparallel dipole configurations (see the arrows on the c domains). In contrast to the open-circuit case, the film surface charge in the short-

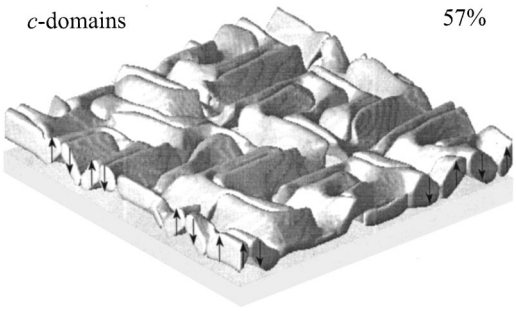

FIG. 1. Domain morphologies with $\bar{\epsilon}=-0.002$ and open-circuit electric condition.

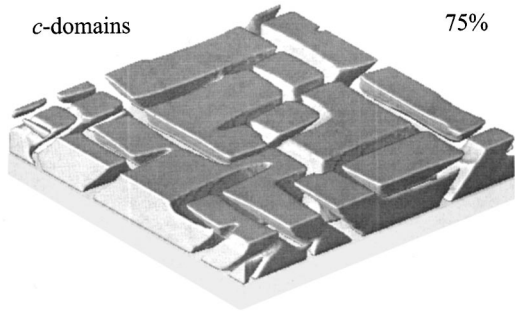

FIG. 3. Domain morphologies with $\bar{\epsilon}=-0.002$, but ignoring electrostatic interaction.

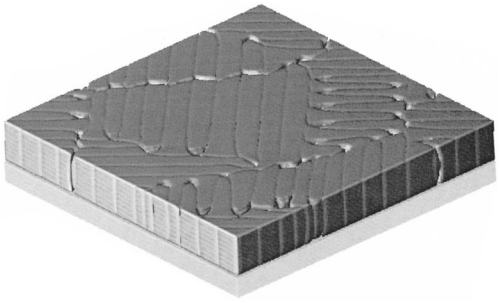

FIG. 4. *a* domain morphology with $\bar{\epsilon}=0.016$ and short-circuit electric condition.

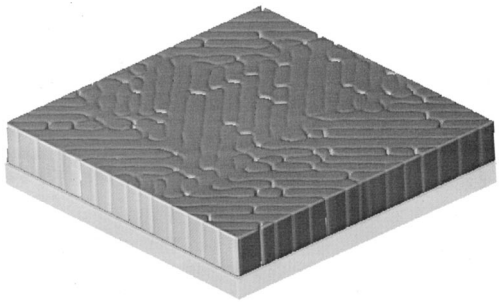

FIG. 5. *a* domain morphology with $\bar{\epsilon}=0.016$, but ignoring electrostatic interaction.

circuit case is compensated, thus, no depolarization field is produced. However, the constant electrical potential on the surfaces in the short-circuit boundary condition promotes the formation of *c* domains. Therefore, the volume fraction of *c* domains increases in the short-circuit condition while decreases in the open-circuit condition. These findings seem to contradict with those in Ref. 25, where the authors concluded that depolarizing fields did not affect the domain structures and volume fractions.

As a second example, we considered a larger tensile substrate constraint $\bar{\epsilon}=0.016$. For both the open-circuit and short-circuit boundary conditions, only a_1 and a_2 domains exist. Since the electric boundary conditions are defined on the film surfaces, their effect on *a*-domain morphology is small, and thus the domain structures for the two electric conditions are similar. Due to the page limit, only the result from the short-circuit condition is presented (Fig. 4) and compared to the case without considering the electrostatic energy at all (Fig. 5). In the *a*-domain structures, the a_1 and a_2 domains are not distinguished but the domain walls are displayed. Although the *a*-domain structures in both Figs. 4 and 5 consist of similar closely packed lamellae, the constant surface electrical potential in the short-circuit boundary condition case results in larger domain sizes. Moreover, the dipole–dipole interactions considered in the short-circuit boundary condition promote head-to-tail or tail-to-head arrangement across the 90° domain walls between a_1 and a_2 domains. In contrast, a random arrangement of head-to-head, tail-to-tail, or head-to-tail configurations is observed in Fig. 5 since the dipole–dipole interaction is ignored. Finally, comb-like or zigzag domain structures are observed in Fig. 4. This is also a consequence of dipole–dipole interactions which prevent two domains of antiparallel polarization to connect with head-to-head or tail-to-tail configurations. Interestingly, such comb-like domain structures or zigzag domain boundaries have been observed in experiments.[26–28]

In summary, a phase-field model for predicting domain structures in a thin film is developed, which allows different mechanical and as well as electrical boundary conditions. Simulation results on a cubic to tetragonal transition in $PbTiO_3$ thin film demonstrate that depolarization field and dipole–dipole interaction can lead to significant changes in domain shapes and domain volume fractions.

The authors are grateful for the financial support from the National Science Foundation under Grant Nos. DMR-0103354, DMR-0122638, and DMR-9983532.

[1] L. E. Cross, *Ferroelectric Ceramics* (Birkhauser, Basel, 1993), pp. 1–85.
[2] D. Damjanovic, Rep. Prog. Phys. **61**, 1267 (1998).
[3] G. H. Haertling, J. Am. Ceram. Soc. **82**, 797 (1999).
[4] A. L. Roytburd and Y. Yu, Ferroelectrics **144**, 137 (1993).
[5] A. L. Roytburd and Y. Yu, in *Twinning in Advanced Materials*, edited by M. H. Yoo and M. Wuttig (TMS, Warrendale, 1994), p. 217.
[6] J. S. Speck and W. Pompe, J. Appl. Phys. **76**, 466 (1994).
[7] B. S. Kwak, A. Erbil, J. D. Budai, M. F. Chisholm, L. A. Boatner, and B. J. Wilkens, Phys. Rev. B **49**, 14865 (1994).
[8] S. Little and A. Zangwill, Phys. Rev. B **49**, 16659 (1994).
[9] C. M. Foster, Z. Li, M. Buckett, D. Miller, P. M. Baldo, L. E. Rehn, G. R. Bai, D. Guo, H. You, and K. L. Merkle, J. Appl. Phys. **78**, 2607 (1995).
[10] S. Stemmer, S. K. Streiffer, F. Ernst, M. Ruhle, W. Y. Hsu, and R. Raj, Solid State Ionics **75**, 43 (1995).
[11] A. Seifert, F. F. Lange, and J. S. Speck, J. Mater. Res. **10**, 680 (1995).
[12] N. Sridhar, J. M. Rickman, and D. J. Srolovitz, Acta Mater. **44**, 4097 (1996).
[13] S. P. Alpay and A. L. Roytburd, J. Appl. Phys. **83**, 4714 (1998).
[14] N. A. Pertsev and V. G. Koukhar, Phys. Rev. Lett. **84**, 3722 (2000).
[15] V. G. Koukhar, N. A. Pertsev, and R. Waser, Appl. Phys. Lett. **78**, 530 (2001).
[16] V. G. Koukhar, N. A. Pertsev, and R. Waser, Phys. Rev. B **64**, 214103 (2001).
[17] A. L. Roytburd, S. P. Alpay, L. A. Bendersky, V. Nagarajan, and R. Ramesh, J. Appl. Phys. **89**, 553 (2001).
[18] Y. L. Li, S. Y. Hu, Z. K. Liu, and L. Q. Chen, Appl. Phys. Lett. **78**, 3878 (2001).
[19] Y. L. Li, S. Y. Hu, Z. K. Liu, and L. Q. Chen, Acta Mater. **50**, 395 (2002).
[20] K. Binder, Ferroelectrics **35**, 99 (1981).
[21] D. R. Tilley and B. Zeks, Solid State Commun. **49**, 823 (1984).
[22] L. Q. Chen and J. Shen, Comput. Phys. Commun. **108**, 147 (1998).
[23] M. J. Haun, E. Furman, S. J. Jang, H. A. Mckinstry, and L. E. Cross, J. Appl. Phys. **62**, 3331 (1987).
[24] N. A. Pertsev, A. G. Zembilgotov, and A. K. Tagantsev, Phys. Rev. Lett. **80**, 1988 (1998).
[25] S. P. Alpay, V. Nagarajan, L. A. Bendersky, M. D. Vaudin, S. Aggarwal, R. Ramesh, and A. L. Roytburd, J. Appl. Phys. **85**, 3271 (1999).
[26] Z. Kighelman, D. Damjanovic, M. Cantoni, and N. Setter, J. Appl. Phys. **91**, 1495 (2002).
[27] S. I. Yakunin, V. V. Shakmanov, G. V. Spivak, and N. V. Vasil'eva, Sov. Phys. Solid State **14**, 310 (1972).
[28] C. A. Randall and D. J. Baraer, J. Appl. Phys. **76**, 925 (1987).